Available online at www.sciencedirect.com

ScienceDirect

Proceedings of the Combustion Institute 37 (2019) 1013–1021

Proceedings of the Combustion Institute

www.elsevier.com/locate/proci

Examination of a soot model in premixed laminar flames at fuel-rich conditions

Warumporn Pejpichestakul [a,b], Eliseo Ranzi [a], Matteo Pelucchi [a], Alessio Frassoldati [a], Alberto Cuoci [a], Alessandro Parente [b,c], Tiziano Faravelli [a,*]

[a] *Department of Chemistry, Materials and Chemical Engineering "G. Natta", Politecnico di Milano, P.zza Leonardo da Vinci 32, 20133 Milano, Italy*

[b] *Université Libre de Bruxelles, Ecole polytechnique de Bruxelles, Aero-Thermo-Mechanics Laboratory, Avenue F.D. Roosevelt, 50 - CP 165/41, 1050 Brussels, Belgium*

[c] *Combustion and Robust Optimization Group (BURN), Université Libre de Bruxelles and Vrije Universiteit Brussel, 1050 Bruxelles, Belgium*

Received 30 November 2017; accepted 13 June 2018
Available online 8 August 2018

Abstract

The primary objective of the present work is to collect and review the vast amount of experimental data on rich laminar premixed flames of hydrocarbon fuels reported in recent years, and to analyze them by using a detailed kinetic mechanism, identifying aspects of the mechanism of PAH and soot formation requiring further revisions. The kinetic assessment was hierarchically conducted, with the progressive extension of the core C_0–C_2 NUIG mechanism up to the CRECK kinetic mechanism of PAH and soot formation. This mechanism is here adopted to evaluate and analyze the extensive amount of experimental data collected. Therefore, it provides a kinetic guideline, useful to critically compare and unify flames involving similar fuels and/or conditions from different sources. The relevant effect of soot particles formation on heavy PAHs concentration is also discussed, together with the kinetic analysis highlighting systematic deviations and critical issues still existing in the present model. The model performances were evaluated using the Curve Matching approach (Bernardi et al., 2016). Considering the challenges of quantitative PAH measurements and associated uncertainties, this extensive database is a further value of this paper and is beneficial for improving reliability of kinetic models in a wide range of conditions.

Keywords: Laminar premixed flames; Experimental database; PAH; Soot precursors

* Corresponding author.
E-mail address: tiziano.faravelli@polimi.it (T. Faravelli).

https://doi.org/10.1016/j.proci.2018.06.104

1. Introduction

Polycyclic aromatic hydrocarbons (PAH) are carcinogenic compounds harmful to human health. In addition to this, PAHs are also precursors of soot by means of radical addition reactions on double bonds, cyclization, and formation of resonantly stabilized radicals, finally resulting in incipient soot [1]. The formation of soot has been intensively studied through different modeling approaches [2–4]. However, all of them require predictive and comprehensive detailed kinetic mechanisms able to correctly describe PAHs formation for a wide range of fuels and operating conditions.

PAH growth and soot formation are typically investigated in nearly sooting or sooting premixed laminar flames [5]. A large number of experimental studies of rich premixed laminar flames have been presented in the past decades, providing a massive amount of detailed information on temperature and concentration profiles for individual flames. The last effort to collect and review several flames for different hydrocarbon fuels dated back to over eight years ago and consisted of 22 flames [6]. Since then, advances in analytical techniques and additional measurements drove improved predictive capabilities of kinetic models. These advancements motivate the comprehensive collection here reported which is used to gain significant insights on current knowledge of PAHs and soot chemistry. This work provides the basis for further improvements of the CRECK soot model by means of a hierarchical approach to the modeling of PAHs kinetics in flames.

The motivations and objectives of the present work are:

(i) To organize an extensive data collection of literature measurements in rich laminar premixed flames of different hydrocarbon fuels;
(ii) To critically assess the model performance through extensive comparisons with experimental data by means of a statistical analysis using the curve matching (CM) approach [7].

Simulations of all the flames are done with the updated CRECK kinetic mechanism of PAH and soot formation [8,9], which includes the reference C_0–C_2 chemistry developed at NUIG [10]. These simulations are useful both for the evaluation of the consistency of experimental data and for identifying limitations in kinetic models. To our knowledge, this work constitutes the first effort toward such an extensive and systematic analysis on PAHs chemistry, also highlighting the effect of soot formation on the yields of intermediate PAHs.

Table 1 summarizes the experimental conditions of the laminar flames here investigated. The database provided in the Supplementary Material (SM) accounts for 60 flames, for more than 20 different C_1–C_{10} fuels, in a wide range of equivalence ratios ($\phi = 1.00$–3.06) and pressures ($P = 0.03$–1.00 atm).

2. Kinetic mechanism and numerical methods

The gas-phase high temperature CRECK mechanism (244 species and ~6000 reactions) implements a C_0–C_3 core mechanism obtained from the H_2/O_2 and C_1/C_2 subsets from Metcalfe et al. [10], C_3 from Burke et al. [11], and heavier fuels from Ranzi et al. [12,13]. This important step toward the unification of core mechanisms allows to more effectively focus the attention on specific features of heavier and more complex molecules such as PAHs. The thermochemical properties were adopted, when available, from the ATcT database of Rusic [14] or from Burcat's database [15]. Unavailable properties of some species were obtained from group additivity method [16]. The kinetic mechanism with thermodynamic and transport properties is attached as Supplementary Material to this study.

With the aim to update the detailed kinetic mechanism towards PAH and soot, the dominant molecular weight growth pathways described according to the HACA mechanism [17], were revised based on the recent theoretical study by Mebel et al. [18]. To fit this detailed and accurate description to the constrained size of the CRECK model [12,13], many isomer species were lumped, where appropriate. Regardless, the relative branching ratios are taken into account in the lumped mechanism, treating reactions with explicit forward and backward rates. In fact, as already discussed elsewhere [8,19], the CRECK mechanism involves only 20 lumped species and 16 radicals for the progressive growth from naphthalene to C_{20} species, which are the first soot precursors (BIN1). Additionally to HACA mechanism, the mass growth through light and heavy resonantly stabilized radicals (from propargyl C_3H_3, up to indenyl (C_9H_7)) is also considered [12].

The soot mechanism, based on a discrete sectional model, is then coupled to the PAH sub-mechanism to describe the evolution from gas-phase to solid particles. The whole range of carbon atoms of heavy PAH and soot particles (from 20 up to more than 10^8 C atoms) is divided into 25 sections with a spacing factor of two. 25 classes of lumped-pseudo species called "BIN" are considered with three different hydrogenation levels. The first four BINs (up to 160 carbon atoms) are heavy PAH, while heavier BINs are soot particles (up to 4×10^4 carbon atoms) and then soot aggregates. Thus, the soot kinetic model involves 150 molecular and radical species for describing the formation of soot particles up to ~0.2 μm, i.e. 3.2×10^8 carbon atoms. The soot kinetic model consists of surface growth, nucleation, coagulation and oxidation processes. The surface growth reactions include

Table 1
Flame database. Experimental conditions and global error index (Ei) calculated using the Curve Matching approach [7].

No.	Fuel	T_{max} (K)	P (atm)	Φ	v_0 (cm/s)[a]	Ei	Ref.
1	CH_4	1600	1.00	2.5	5.24	0.33	Marinov et al. [27]
2	CH_4	1776	1.00	2.4	5.00	0.24	Alfè et al. [31]
3–5	CH_4	1682–1709	1.00	2.2–2.6	5.35	0.31	Melton et al. [24]
6–7	CH_4	1805–1850	0.26	2.1–2.3	8.55	0.4	El Bakali et al. [32]
8–9	CH_4/H_2	1683–1701	1.00	2.2–2.4	5.90–6.20	0.25	Mze Ahmed et al. [33]
10	C_2H_2	1850	0.03	2.5	97.00	0.24	Bastin et al. [34]
11	C_2H_2	1901	0.03	2.4	50.00	0.25	Westmoreland et al. [35]
12	C_2H_2	1992	0.12	2.8	20.40	0.34	Bockhorn et al. [36]
13	C_2H_2	1912	0.03	2.25	63.08	0.31	Li et al. [37]
14	C_2H_2	2121	0.04	2.4	58.95	0.29	Bierkandt et al. [38]
15–16	C_2H_2/C_3H_4-A	2200–2300	0.03	1.7–2.4	72.75	0.21	Miller et al. [39]
17	C_2H_4	1430	1.00	3.1	6.42	0.45	Castaldi et al. [40]
18	C_2H_4	1600	1.00	2.8	6.84	0.21	Harris et al. [41]
19–20	C_2H_4	1592–1610	1.00	1.5–1.9	3	0.42	Barbella et al. [42]
21–23	C_2H_4	1552–1818	1.00	2.4	2–6	0.33	Ciajolo et al. [43]
24	C_2H_4	1710	1.00	2	5.87	0.38	Carbone et al. [25]
25	C_2H_4	1574	1.00	2.8	4.90	0.32	Migliorini et al. [44]
26–28	C_2H_4	1556–1643	1.00	2.3–2.9	6.73	0.51	Xu et al. [27]
29	C_2H_4	2192	0.03	1.9	62.5	0.33	Bhargava et al. [45]
30	C_2H_6	1600	1.00	2.5	6.37	0.34	Marinov et al. [27]
31–34	C_2H_6	1681–1800	1.00	2–2.6	6.19–7.26	0.38	Melton et al. [26]
35–36	C_3H_4	2185–2262	0.03	1.8	48.2	0.28	Hansen et al. [46]
37	C_3H_6	2306	0.05	2.3	50.00	0.23	Bohm et al. [47]
38	C_3H_8	1250	1.00	2.5	4.77	0.35	Marinov et al. [48]
39	C_4H_6	2050	0.03	2.4	50.00	0.28	Cole et al. [49]
40	NC_4H_{10}	1600	1.00	2.6	6.38	0.4	Marinov et al. [50]
41–44	CYC_5H_8	2098–2168	0.05	1.7-2.6	50–54.7	0.3	Lamprecht et al. [51], Hansen et al. [52]
45	C_6H_6	1905	0.03	1.8	50.00	0.24	Bittner et al. [53]
46–48	C_6H_6	1778–2101	0.04	1.25–2	36.10	0.25	Yang et al. [54]
49–50	C_6H_6	1742–1850	1.00	1.8–1.9	4.00	0.42	Tregrossi et al. [55]
51–52	C_6H_6	1720–1810	1.00	2	3-4	0.31	Russo et al. [56]
53–54	C_6H_6	1722–1885	0.05	2	35–40.5	0.28	Vandooren et al. [57][58]
55	C_6H_6/CH_4	1500	0.05	1	1.8	0.23	El Bakali et al. [59]
56	CYC_6H_{12}	1752	1.00	2. 3	4.00	0.29	Ciajolo et al. [60]
57	C_7H_8	1743	0.05	2.00	40.50	0.26	Detilleux et al. [61]
58-59	NC_7H_{16}/IC_8H_{18}	1614	1.00	1.9	4.12-4.98	0.19	El Bakali et al. [62]
60	$C_{10}H_8$	1860	0.03	1.7	50.00	0.34	Griesheimer et al. [63]

[a] Cold gas velocity.

HACA mechanism, as well as gaseous species and PAH condensation reactions. The condensing species are molecules and radicals of aromatic starting from benzene and phenyl radical. The complete soot sub-mechanism consists of ∼400 species and 25,000 reactions. Further details on the soot model are available in [8,9].

2.1. Numerical methods

Numerical simulations were performed using the 1-D laminar flame solver implemented in the OpenSMOKE++ suite of programs [20]. The mixture-average diffusion coefficient was used in the simulation. Thermal diffusion (Soret effect) is also included in species transport equations. Solution gradient and curvature coefficients of 0.05 and 0.5 were assigned to ensure the smoothness of the calculated profiles. The measured temperature profiles were imposed to the simulations to account for the unknown conductive and radiative heat losses.

2.2. Curve Matching and performance evaluation

Assessing the overall performances of the kinetic model over the wide set of experimental flames is a challenging task, because of the large number of species profiles. The Curve Matching approach [7] was here adopted to evaluate the agreement between experimental data and model predictions. It performs quantitative and qualitative error comparisons by the transformation of discrete experimental data and model predictions into two different continuous functions. It provides individual error indices, which account not only for square errors, but also for the shape of the species profiles. An integrated error index (E_{flame}) of each flame (average over all species) and an in-

tegrated error index ($E_{species}$) of each species (average over all flames) are also provided. Error indices range between 0 (accurate model) and 1 (inaccurate model).

3. Results

Before discussing PAHs formation in sooting flames, it is first important to assess the model reliability in predicting the main combustion features of key PAH precursors such as cyclopentadiene and single ring aromatics. Comparisons of model predictions with experimental data for the laminar flame speed of acetylenic species, cyclopentadiene, benzene and toluene are therefore reported in the SM. These comparisons confirm and emphasize the role of resonantly stabilized radicals in reducing laminar flame speed [12]. The interest in cyclopentadienyl radical is also due to its role in naphthalene formation through self-recombination reactions. Moreover, the interest in phenyl radical chemistry is due to its relevance in the HACA mechanism.

All the 60 flames were simulated, with and without the soot sub-mechanism, and detailed results and comparisons with the experimental measurements are reported in the SM. As reported in Table 1, the integrated error index (Ei) varies from ~0.15 in the case of n-heptane (Flame 58), up to >0.5 for ethylene Flame 26, indicating a very poor predictive capability. A preliminary analysis of the error index trend does not seem to indicate systematic deviations depending on fuels, equivalent ratios, or soot yields. Due to space limitations, in the attempt to obtain the most significant, effective and general overview, scatter plots between the maximum predicted and measured value of measured species are here reported as a global measure of model performances, together with the error index of each species. The SM contains the complete set of comparisons, also grouping the same species in different flames.

3.1. Major species formation in flames

Figure 1 shows the parity diagrams of maximum experimental and predicted concentrations of major species in rich flames, for different fuels. As expected, CO is the primary component in rich conditions. Predicted CO profiles agree within 20% with the measurement and do not show systematic deviations. The model captures CO_2 predictions quite well, also for $C_6H_6/O_2/Ar$ at $\phi = 1.25$ (Flame 46, Yang et al., 2015), where CO is largely converted to CO_2, after reaching its maximum concentration. A similar degree of accuracy is found for H_2 and H_2O, even if larger deviations are observed in most of CH_4 flames where both species are under-predicted.

The scatter diagrams of CH_4 and the sum of C_2H_4 and C_2H_2 are also satisfactory. Larger uncertainties are indeed observed for the parity diagrams of individual species C_2H_4 and C_2H_2, as reported in the SM. Similar deviations are also observed using other literature models [21,22]. Although C_2H_2 predictions are more accurate for atmospheric flames, more scattered results are observed at lower pressures, where over- or under-predictions up to a factor of ~3 are highlighted. C_2H_4 seems systematically over-predicted in CH_4 and C_2H_6 flames, highlighting shortcomings in both C_2H_6 formation and dehydrogenation pathways within the C_0–C_2 mechanism. C_3H_4s (propyne and allene) and benzene are correctly predicted by the model, whereas diacetylene (C_4H_2), despite its lower concentration, deserves greater attention.

Large under-predictions of C_4H_2 are in fact observed in atmospheric flames, whereas minor discrepancies are obtained at low pressures. Similar disagreements are observed with KAUST [21] and Blanquart et al. [22] mechanisms (see SM). The lack of consistent findings, together with the possible relevance of C_4H_2 in soot formation mechanism, suggests the need of further investigating acetylenic species kinetics.

3.2. Heavier aromatics and PAHs formation in flames

Figure 2 shows the scatter plots of PAHs clearly highlighting the higher propensity of C_{3+} fuels to form heavier species. The overall prediction of PAHs in atmospheric flames is satisfactory, but most of the low-pressure benzene flames show an overestimation of phenylacetylene ($C_6H_5C_2H$) and underestimation of naphthalene ($C_{10}H_8$). Similar deviations are also obtained with [21] and [22] (see SM). This suggests that pressure dependent rates of acetylene addition might require further revision.

It has to be noted that Fig. 2 shows the scatter plots of heavier species as predicted with the complete kinetic mechanism, also including the soot model. Together with the previous comments on the observed deviations at low pressures, it is worth noting the general over-predictions, at high pressures. The lumping of heavy species can partially explain these deviations. In facts, lumped phenanthrene groups not only anthracene, but also C_{13} and C_{15} homologous species.

Figure 3 shows the error index of different species, as averaged over the different flames, versus the number of available data. The convergent behavior suggests the importance of the number of measurements to improve model reliability. Good predictive capabilities are shown for benzene and gaseous species for which not only the availability of many reliable data, but also the information gained from quantum chemistry ensure a deeper knowledge.

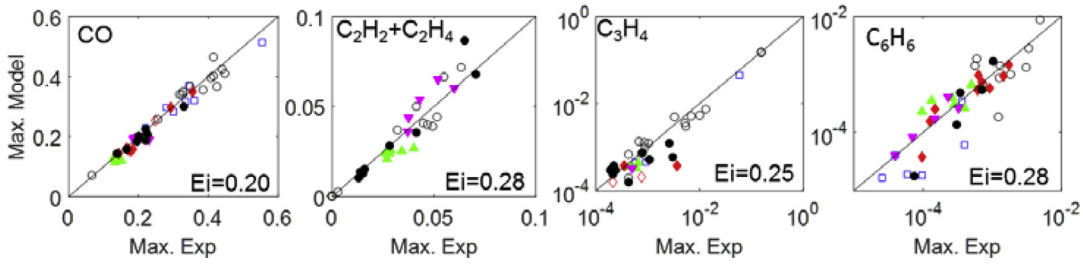

Fig. 1. Scatter plots of the maximum calculated and measured concentration of major species. Each marker represents main fuels, Δ:CH_4, □: C_2H_2, ◇: C_2H_4, ▽: C_2H_6, and ○: C_{3+}. Void symbol: low-pressure flames. Filled symbol: atmospheric flames.

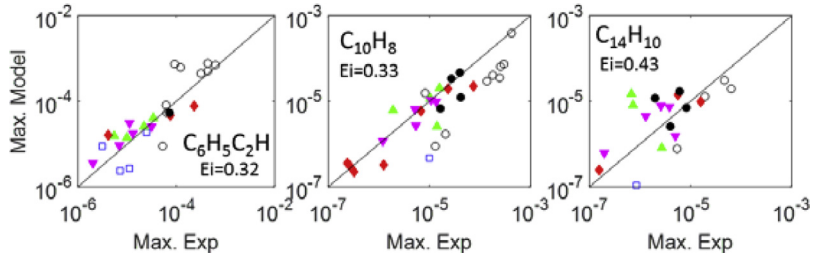

Fig. 2. Scatter plots of maximum experimental and predicted concentration of phenylacetylene, naphthalene, and phenanthrene. Symbols as in Fig. 1.

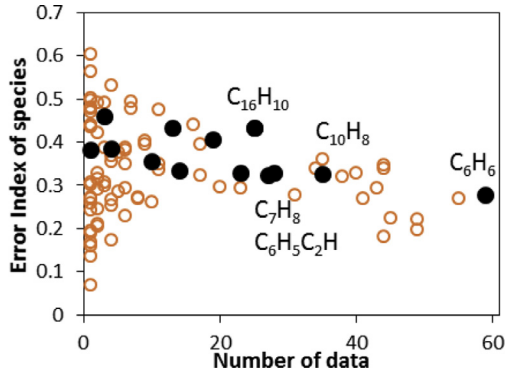

Fig. 3. Error index of different species. Filled symbol: aromatic species. Void symbol: gaseous species.

3.3. *Effect of soot on PAH predictions*

Although it is intuitive that accounting for soot formation leads to a reduction of PAH concentration [23], the scope of this section is to quantify this effect, by comparing model predictions with and without soot mechanism. Figure 4 clearly shows this relevant effect on benzene profiles from CH_4 [24], C_2H_4 [25], and C_2H_6 [26] flames. The inclusion of the soot significantly reduces not only the maximum but the entire benzene yields along the space domain (dashed lines in Fig. 4), with an improved agreement in all the three cases.

Soot presence affects the benzene yield in Flame 4 and 5 ($CH_4/O_2/Ar$ – $\phi = 2.4$–2.6 – Melton et al. [24]). On the contrary, this effect is negligible when considering the benzene formation in Flame 1 ($CH_4/O_2/Ar$ – $\phi = 2.5$ – Marinov et al. [27]), as reported in the SM. By comparing the temperature profiles of these flames, it is possible to note that the maximum temperature of Flame 1 ($T_{max} = 1600$ K) is about 100 K lower than the maximum temperature of Flames 4 and 5, even though the flame conditions are very similar. By correcting and assuming a higher flame temperature profile for Flame 1, it is possible to observe the soot influence and to achieve a better agreement with experimental data (see SM). This critical analysis of the consistency of similar flames shows one of the useful aspects of the database.

Relevant variations of $C_{10}H_8$ and mainly of heavier PAHs are also observed, as reported in the SM. Figure 5 shows the predicted reduction of the error index of major PAH in sooting flames at different equivalence ratios. The reduction percentage is calculated by comparing error indices with and without soot model. As expected, the soot chemistry allows to reduce the average error indices, with average reductions of about 10%, increasing at richer conditions. The 33% reduction of the error index of pyrene at $\phi = 2$ – Flame 31 [26] is not very significant, because of its very low concentration (<1 ppm). Close to non-sooting conditions the differences decrease to less than 1%. The blue line shows the average reduction of error in-

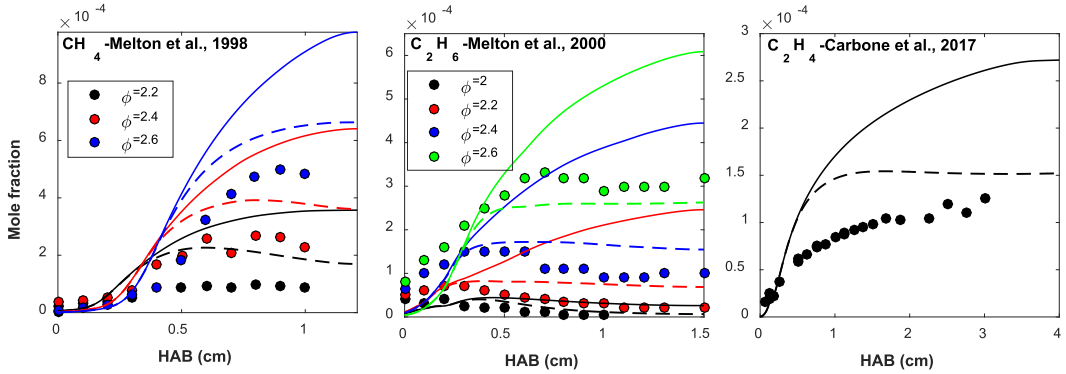

Fig. 4. Comparison between experimental (symbols) and predicted $C_{10}H_8$ profiles. Model predictions with (dashed lines) and without soot kinetic model (solid lines). Left panel: CH_4 flames (Flames 3–5) [24]. Middle panel: C_2H_6 flames (Flames 31–34) [25]. Right panel: C_2H_4 flames (Flame 24) – $\phi = 2$ [26].

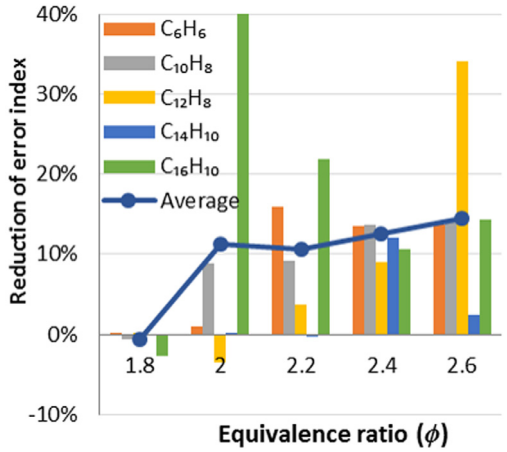

Fig. 5. Reduction of error index of intermediate PAHs at different equivalence ratio. (For interpretation of the references to color in this figure legend, the reader is referred to the web version of this article.)

dex, increasing for higher soot propensity conditions (i.e. higher equivalence ratios). This improvement in error index confirms the important role of PAH condensation and soot growth processes.

Additionally, the model performance evaluation suggests that validation of PAH without the soot sub-mechanism is misleading, particularly in rich flames. As demonstrated in [3], the coupling of different PAH mechanisms to the same soot model provides significantly different predictions. The database reported herein is also useful for the selection of the most appropriate PAH mechanism and for the verification of PAH consumption by soot model.

To verify the overall performances of the model in predicting soot volume fraction, Fig. 6 shows a comparison with data collected in CH_4 and C_2H_6 flames by Melton et al. [24,26], as well as in the C_2H_4 flame of Carbone et al. [25]. Good agreement is observed for CH_4 and C_2H_6 flames. While soot volume fraction from CH_4 is consistently under-predicted mainly for short distances from the burner, for the ethane cases a better agreement is observed, with maximum deviations of a factor of ~2 for the intermediate $\phi = 2.4$ case. A reasonable agreement with the experimental data is observed in the C_2H_4 flame of Carbone et al. [25].

The overall reasonable agreement between experimental data and model predictions allows to rely on the analysis of the PAH-soot interaction through the surface growth reactions. Figure 7 schematically shows the relative contributions of HACA mechanism and PAH condensation reactions to the formation and growth of soot particles, obtained from the soot model at different pressures. Acetylene is mostly involved in the HACA mechanism with the growing of PAH species. At atmospheric pressure, incipient soot particles form near flame region and react with aromatic radicals via chemical condensation. PAHs also interacts with soot particles, in the post-flame region. Thus, the role of C_2H_2 and HACA mechanism in the successive soot growth decreases, because of the preferential addition to most abundant PAH than to the heavy particles present in lower concentrations. Mainly in very rich flames at high pressure, benzene and heavy PAHs condensation reactions on soot particles play a relevant role. Because of their relative concentration, benzene contribution is the dominant one, followed by phenylacetylene and naphthalene. At lower pressure instead, acetylene addition dominates over PAH condensation, as PAH concentration strongly depends on pressure [18]. This pressure effect is in agreement with the observations with Guo et al. [28]. However, the different relative role at atmospheric condition from this work is due to the concerned PAH in the model and PAH chemistry. In addition to pressure, the two competitive pathways depend on temperature and equivalence ratio. In particular, lower

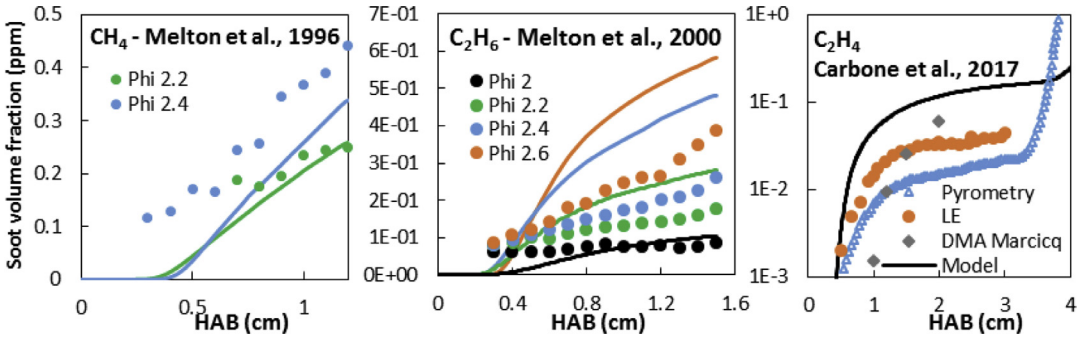

Fig. 6. Comparison between predicted (lines) and measured (symbols) soot volume fraction in different flames.

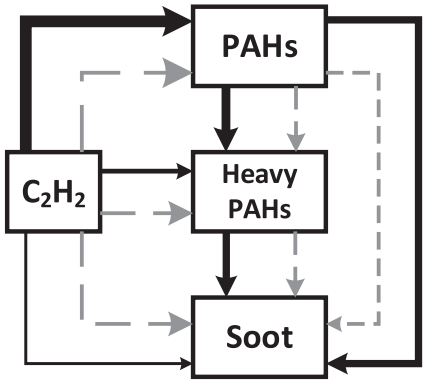

Fig. 7. Relative contributions of HACA mechanism and PAH condensation reactions to the growth of soot particles at low (dashed lines) and atmospheric pressure (solid lines). The thickness of the arrows represents the importance of the different paths.

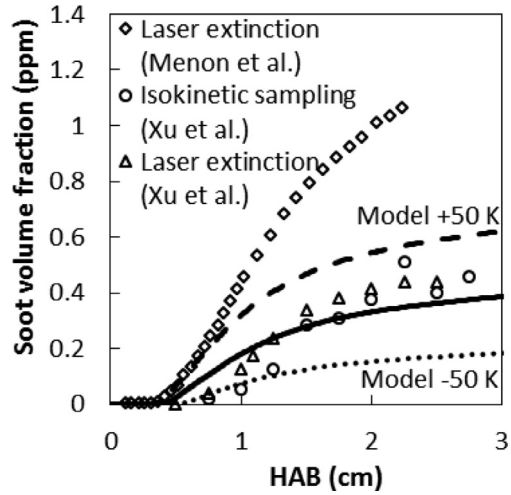

Fig. 8. Temperature effect on soot formation of C_2H_4 flame (Flame 27) [29,30]. Comparison of measured (symbols) and predicted (lines) soot volume fraction.

temperatures and higher equivalent ratios increase the relative role of PAH condensation compared to C_2H_2 addition. Mainly in methane and ethane flames, it is important to highlight that acetylene is also involved in benzene formation, via the methyl addition to form propargyl radical.

3.4. Experimental uncertainties and temperature effect on soot predictions

Accurate experimental temperatures are crucial for kinetic studies especially in rich flames where soot fouling and disturbances can affect measurements [27]. Flame 27 (C_2H_4) [29,30] is chosen to demonstrate the temperature effect. The simulated temperature profile is obtained from Menon et al. [30] that used a spectral line reversal technique up to ~10 mm and two-color pyrometry technique, where the presence of soot perturbs the substantial absorption of radiation from the lamp. This confirms the challenges of accurately measuring temperatures in sooting conditions.

Figure 8 shows the comparison between measurements and model predictions. The model satisfactorily agrees with the experimental measurements when using the original temperature profile. Model predictions obtained perturbing the temperature profile of ±50 K are also reported. These temperature variations strongly impact soot formation. At higher temperatures, soot volume fraction increases of a factor of ~2. This is justified by higher yields of C_2H_2 from C_2H_4 dehydrogenation, enhancing PAHs production. Conversely, the sooting tendencies decrease with temperature. These results highlight the importance of accurate temperature measurements. Besides the obvious impact of temperature on kinetics, thermodynamic effect is also expected on PAH and soot formation at high temperatures.

4. Conclusions

The upgraded CRECK kinetic model, hierarchically obtained by assembling the C_0-C_2 NUIG mechanism [10], the kinetic mechanism of heavy

fuel combustion including PAH formation [12], and the soot model [8,9]was used to simulate the whole set of rich laminar premixed flames. Besides the important steps toward a unified core mechanism, this extensive validation provides a significant overview of the current understanding of the molecular weight growth kinetics leading to nanoparticle formation under high-temperature sooting conditions. The flame database extends the previous one of laminar premixed flame speeds [12], and constitutes an added value to this work and a valuable source of information for the whole combustion community. Moreover, the overall kinetic mechanism including soot formation is furtherly validated over this database, and is provided as Supplementary Material. This comprehensive validation shows regions of fuels/conditions where model predictions are quite accurate (CO, CO_2, H_2, C_2H_2, C_6H_6, etc.) and more importantly, highlights areas requiring further attention (C_4H_2 and other polyyne species). This mechanistic study clearly highlights the important role of PAHs as surface growth species, largely contributing to the successive soot formation. The effect of the soot formation model was also quantitatively investigated, highlighting its importance on heavy PAHs concentrations. The reduction in the average error index of intermediate PAHs shows that neglecting the successive soot formation leads to deviations up to 10%. The better qualitative and quantitative agreement obtained by using the complete kinetic model proves that the soot sub-mechanism is necessary to properly analyze rich sooting flames.

Finally, this paper demonstrates that not only kinetic model uncertainties and simplifications, but also experimental uncertainties in temperature and PAHs measurements significantly affect predicted soot yields. Therefore, more significant insights can only be obtained from a comprehensive mechanism validation relying on all the possible target flames, coming from different facilities, for different fuels and experimental conditions.

Acknowledgments

This project has received funding from the European Union's Horizon 2020 research and innovation programme under the Marie Sklodowska-Curie grant agreement No. 643134.

Supplementary materials

Supplementary material associated with this article can be found, in the online version, at doi:10.1016/j.proci.2018.06.104.

References

[1] H. Wang, *Proc. Combust. Inst.* 33 (2011) 41–67.
[2] M.E. Mueller, G. Blanquart, H. Pitsch, *Combust. Flame* 156 (2009) 1143–1155.
[3] A. Veshkini, N.A. Eaves, S.B. Dworkin, M.J. Thomson, *Combust. Flame* 167 (2016) 335–352.
[4] E.K.Y. Yapp, D. Chen, J. Akroyd, et al., *Combust. Flame* 162 (2015) 2569–2581.
[5] C.S. McEnally, L.D. Pfefferle, B. Atakan, K. Kohse-Höinghaus, *Prog. Energy Combust. Sci* 32 (2006) 247–294.
[6] H.R. Zhang, E.G. Eddings, A.F. Sarofim, C.K. Westbrook, *Proc. Combust. Inst.* 32 (2009) 377–385.
[7] M.S. Bernardi, M. Pelucchi, A. Stagni, et al., *Combust. Flame* 168 (2016) 186–203.
[8] C. Saggese, S. Ferrario, J. Camacho, et al., *Combust. Flame* 162 (2015) 3356–3369.
[9] W. Pejpichetsakul, A. Frassoldati, A. Parente, T. Faravelli, in: Tenth Mediterranean Combustion Symposium, Naples, Italy, 2017.
[10] W.K. Metcalfe, S.M. Burke, S.S. Ahmed, H.J. Curran, *Int. J. Chem. Kinet* 45 (2013) 638–675.
[11] S.M. Burke, U. Burke, R. Mc Donagh, et al., *Combust. Flame* 162 (2015) 296–314.
[12] E. Ranzi, A. Frassoldati, R. Grana, et al., *Prog. Energy Combust. Sci* 38 (2012) 468–501.
[13] E. Ranzi, A. Frassoldati, A. Stagni, M. Pelucchi, A. Cuoci, T. Faravelli, *Int. J. Chem. Kinet.* 46 (2014) 512–542, doi:10.1002/kin.20867.
[14] B. Ruscic, *J. Phys. Chem. A* 119 (2015) 7810–7837.
[15] E. Goos, A. Burcat, B. Ruscic, *Extended Third Millenium Ideal Gas Thermochemical Database with updates from Active Thermochemical Tables* (2017). http://burcat.technion.ac.il/dir mirrored at http://garfield.chem.elte.hu/Burcat/burcat.html.
[16] S.W. Benson, F. Cruicksh, D.M. Golden, *Chem. Rev.* 69 (3) (1969) 279–324.
[17] M. Frenklach, H. Wang, in: H. Bockhorn (Ed.), Soot Formation in Combustion: Mechanisms and Models of Soot Formation, Springer Series in Chemical Physics, vol. 59, Springer-Verlag, Berlin, 1994, pp. 162–190.
[18] A.M. Mebel, Y. Georgievskii, A.W. Jasper, S.J. Klippenstein, *Proc. Combust. Inst.* 36 (2017) 919–926.
[19] A. Frassoldati, G. D'Errico, T. Lucchini, et al., *Combust. Flame* 162 (2015) 3991–4007.
[20] A. Cuoci, A. Frassoldati, T. Faravelli, E. Ranzi, *Comput. Phys. Commun.* 192 (2015) 237–264.
[21] Y. Wang, A. Raj, S.H. Chung, *Combust. Flame* 160 (2013) 1667–1676.
[22] G. Blanquart, P. Pepiot-Desjardins, H. Pitsch, *Combust. Flame* 156 (2009) 588–607.
[23] M.R. Djokic, K.M. Van Geem, C. Cavallotti, A. Frassoldati, E. Ranzi, G.B. Marin, *Combust. Flame* 161 (2014) 2739–2751.
[24] T.R. Melton, A.M. Vincitore, S.M. Senkan, *Symp. Combust.* 27 (1998) 1631–1637.
[25] F. Carbone, K. Gleason, A. Gomez, *Combust. Flame* 181 (2017) 315–328.
[26] T.R. Melton, F. Inal, S.M. Senkan, *Combust. Flame* 121 (2000) 671–678.
[27] N.M. Marinov, W.J. Pitz, C.K. Westbrook, M.J. Castaldi, S.M. Senkan, *Combust. Sci. Technol.* 116–117 (1996) 211–287.
[28] H. Guo, Z. Gub, K.A. Thomson, G.J. Smallwood, F.F. Baksh, *Proc. Combust. Inst.* 34 (2013) 1795–1802.
[29] F. Xu, P.B. Sunderland, G.M. Faeth, *Combust. Flame* 108 (1997) 471–493.

[30] A.V. Menon, S.-Y.Y. Lee, M.J. Linevsky, T.A. Litzinger, R.J. Santoro, *Proc. Combust. Inst.* 31 (2007) 593–601 I.
[31] M. Alfè, B. Apicella, J.N. Rouzaud, A. Tregrossi, A. Ciajolo, *Combust. Flame* 157 (2010) 1959–1965.
[32] A. El Bakali, X. Mercier, M. Wartel, F. Acevedo, I. Burns, L. Gasnot, J.F. Pauwels, P. Desgroux, *Energy* 43 (2012) 73–84.
[33] A. Mze Ahmed, S. Mancarella, P. Desgroux, L. Gasnot, J.F. Pauwels, A. El Bakali, *Int. J. Hydrogen Energy* 41 (2016) 6929–6942.
[34] E. Bastin, J.L. Delfau, M. Reuillon, C. Vovelle, J. Warnatz, *Symp. Combust.* 22 (1989) 313–322.
[35] P.R. Westmoreland, A.M. Dean, J.B. Howard, J.P. Longwell, *J. Phys. Chem.* 93 (1989) 8171–8180.
[36] H. Bockhorn, F. Fetting, A. Heddrich, G. Wannemacher, *Symp. Combust.* 20 (1985) 979–988.
[37] Y. Li, L. Zhang, Z. Tian, T. Yuan, K. Zhang, B. Yang, F. Qi, *Proc. Combust. Inst.* 32 (2009) 1293–1300.
[38] T. Bierkandt, T. Kasper, E. Akyildiz, A. Lucassen, P. Oßwald, M. Köhler, P. Hemberger, *Proc. Combust. Inst.* 35 (2015) 803–811.
[39] J.A. Miller, J.V. Volponi, J.-F. Pauwels, *Combust. Flame* 105 (1996) 451–461.
[40] M.J. Castaldi, N.M. Marinov, C.F. Melius, J. Huang, S.M. Senkan, W.J. Pit, C.K. Westbrook, *Symp. Combust.* 26 (1996) 693–702.
[41] S. Harris, A. Weiner, *Combust. Sci. Technol.* 31 (1983) 155–167.
[42] R. Barbella, A. Ciajolo, A. D'Anna, A. Tregrossi, in:, Joint Meeting of The Italian and Portuguese Sections of The Combustion Institute, Salsomaggiore Terme, Italy, 1994, p. III-13.
[43] A. Ciajolo, A. D'anna, R. Barbella, A. Tregrossi, A. Violi, *Symp. Combust.* 26 (1996) 2327–2333.
[44] F. Migliorini, S. De Iuliis, F. Cignoli, G. Zizak, *Combust. Flame* 153 (2008) 384–393.
[45] A. Bhargava, *P.R. Westmoreland* (1998) 2180.
[46] N. Hansen, J.A. Miller, C.A. Taatjes, J. Wang, T.A. Cool, M.E. Law, P.R. Westmoreland, *Proc. Combust. Inst.* 31 (2007) 1157–1164.
[47] H. Böhm, A. Lamprecht, B. Atakan, K. Kohse-Höinghaus, *Phys. Chem. Chem. Phys.* 2 (2000) 4956–4961.
[48] N.M. Marinov, M.J. Castaldi, C.F. Melius, W. Tsang, *Combust. Sci. Technol.* 128 (1997) 295–342.
[49] J.A. Cole, J.D. Bittner, J.P. Longwell, J.B. Howard, *Combust. Flame* 56 (1984) 51–70.
[50] N.M. Marinov, W.J. Pitz, C.K. Westbrook, A.M. Vincitore, M.J. Castaldi, S.M. Senkan, C.F. Melius, *Combust. Flame* 114 (1998) 192–213.
[51] A. Lamprecht, B. Atakan, K. Kohse-Höinghaus, *Proc. Combust. Inst.* 28 (2000) 1817–1824.
[52] N. Hansen, T. Kasper, S.J. Klippenstein, P.R. Westmoreland, M.E. Law, C.A. Taatjes, K. Kohse-Höinghaus, J. Wang, T.A. Cool, *J. Phys. Chem. A* 111 (2007) 4081–4092.
[53] J.D. Bittner, J.B. Howard, *Symp. Combust.* 18 (1981) 1105–1116.
[54] J. Yang, L. Zhao, W. Yuan, F. Qi, Y. Li, *Proc. Combust. Inst.* 35 (2015) 855–862.
[55] A. Tregrossi, A. Ciajolo, R. Barbella, *Combust. Flame* 117 (1999) 553–561.
[56] C. Russo, F. Stanzione, A. Tregrossi, M. Alfè, A. Ciajolo, *Combust. Flame* 159 (2012) 2233–2242.
[57] F. Defoeux, V. Dias, C. Renard, P.J. Van Tiggelen, J. Vandooren, *Proc. Combust. Inst.* 30 (2005) 1407–1414.
[58] V. Detilleux, J. Vandooren, *Combust. Explos. Shock Waves* 45 (2009) 392–403.
[59] A. El Bakali, M. Ribaucour, A. Saylam, G. Vanhove, E. Therssen, J.F. Pauwels, *Fuel* 85 (2006) 881–895.
[60] A. Ciajolo, A. Tregrossi, M. Mallardo, T. Faravelli, E. Ranzi, *Proc. Combust. Inst.* 32 I (2009) 585–591.
[61] V. Detilleux, J. Vandooren, *Proc. Combust. Inst.* 33 (2011) 217–224.
[62] A. El Bakali, J.L. Delfau, C. Vovelle, *Combust. Sci. Technol.* 140 (1998) 69–91.
[63] J. Griesheimer, K.-H. Homann, *Symp. Combust.* 27 (1998) 1753–1759.